UAV Bridge Inspection through Evaluated 3D Reconstructions

Siyuan Chen[a], Debra F. Laefer[b], Eleni Mangina[c], Iman Zolanvari[d], Jonathan Byrne[e]

[a] Univ. College Dublin, School of Civil Engineering, Urban Modelling Group, Belfield, Dublin 4, IE

[b] New York Univ., Center for Urban Science + Progress, 370 Jay St., 12th Fl, Brooklyn, NY 11201

[c] Univ. College Dublin, School of Computer Science, Belfield, Dublin 4, Ireland

[d] Univ. College Dublin, School of Civil Engineering, Urban Modelling Group, Belfield, Dublin 4, IE

[e] Univ. College Dublin, School of Civil Engineering, Urban Modelling Group, Belfield, Dublin 4, IE

* Corresponding Author: debra.laefer@nyu.edu

Abstract

Imagery-based, three-dimensional (3D) reconstruction from Unmanned Aerial Vehicles (UAVs) holds the potential to provide safer, more economical, and less disruptive bridge inspection. In support of those efforts, this paper proposes a process using an imagery-based point cloud. First, a bridge inspection procedure is introduced, including data acquisition, 3D reconstruction, data quality evaluation, and subsequent damage detection. Next, evaluation mechanisms are proposed including checking data coverage, analysing points distribution, assessing outlier noise, and measuring geometric accuracy. In this final aspect, the "Guide to the Expression of Uncertainty in Measurement" was used. The overall approach is illustrated in the form of a case study with a low-cost UAV. Areas of particular coverage difficulty involved slim features such as railings, where obtaining sufficient features for image matching proved challenging. Shadowing and large tilt angles hid or weakened texturing surfaces, which also interfered with the matching process.

Introduction

Bridges are important infrastructure components that must be properly maintained to ensure public safety and for which regular inspection is a critical component. Inspection approaches are to some extent dictated by local practice. For example, Ireland's I-STR-6510 requires "ground level inspections" be conducted every two years and a "thorough inspection" once every six years (RAIU 2010). In the United Kingdom (UK), a "general inspection" should be undertaken every one to three years according to the standard "Examination of Bridges and Culverts NR/SP/CIV/017" (Sterritt 2009). Similarly, in the United States (US), a bridge should be inspected every two years according to the American Association of State Highway and Transportation Officials (AASHTO) requirement (AASHTO 1970). Traditionally when inspecting bridges, there is a choice between using an Aerial Work Platform (AWP), an under-bridge inspection vehicle, ladders, or ropes for access. Irrespective of the method used, the associated costs and dangers remain challenges. AWPs and inspection vehicles are likely to require road lane closures, and the equipment used is expensive to maintain and run, while ropes require a high level of training and expertise to be used safely. To date, there has yet to be a rapid and cost-effective method that does not require bridge closure and is able to generate a permanent record. To address that deficit, this paper considers the feasibility and limitations of using an unmanned aerial vehicle (UAV) for documentation from which subsequent inspection can be conducted through a three-dimensional (3D) reconstruction. The paper presents recent efforts in this area followed by a new evaluation framework for 3D reconstruction. The usefulness and importance of this evaluation framework is shown in a case study that demonstrates the proposed workflow for data acquisition, model reconstruction, and data quality determination.

Inspection Approaches

Currently, visual inspection is the primary form of bridge inspection. This may involve in-person inspection, fixed sensors, or camera-based monitoring. Since each has its limitations, significant interest has emerged in using UAVs, as a means to provide faster, cheaper, safer, and more flexible data acquisition, along with generation of an objective digital record, instead of in-person visual assessment, as reported in recent state-of-the-art reviews by Chen et al. (2016) and Hassanalian and Abdelke (2017). The following concentrates on recent efforts to use remote sensing for inspection.

Remote Sensors and Camera-based Inspection

Remote sensors and camera-based inspection can provide continuous bridge evaluation data through permanent deployment, thereby minimizing the safety problems of in-person inspections and the impacts of affiliated bridge closures. To this end, Jahanshahi et al. (2011) introduced an image-based system for bridge inspection (Figure 1a) where on-site imagery was transmitted via cable to an off-site database, and a computer-vision based process was used to reduce inconsistencies in individual inspections. At a working distance of 3 m, with a Canon PowerShot A610 digital camera, the reported minimum measurable feature was 0.57mm. However, the high costs and relatively fixed inspection ranges affiliated with stationary cameras continue to curtail the popularity of this approach. According to a report published by the Minnesota Department of Transportation (Lueker and Marr 2014), the cost for setting up a continuous bridge monitoring system is around $25,000 for the first year with $1,000 per year for annual maintenance.

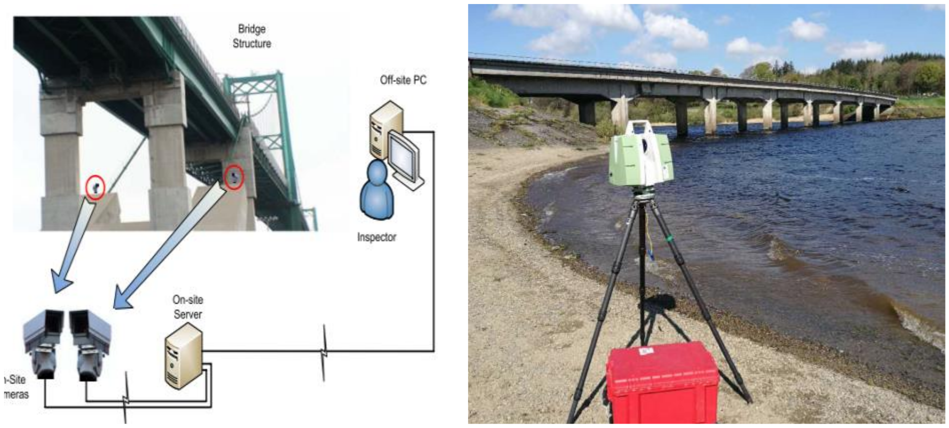

Fig. 1. Remote sensors and cameras inspection. (a) Camera inspection (Jahanshahi et al. 2011); (b) Terrestrial laser scanner (TLS)

To use such a monitoring system in a more efficient way, mobile devices have been developed and deployed. Examples include the work by Nishimura et al. (2012) where a hybrid camera system was fixed atop a moving vehicle This system combined a fixed angle camera for detailed detection and a 360-degree camera for panoramic data recording. However, this system can only be applied in vehicle-accessible areas and is, thus, not fit for underbridge inspection or for documenting distant features such as cables and towers. Terrestrial laser scanning (TSL) is another commonly used approach that can provide high-quality 3D data for bridge damage detection, such as surface loss or cracks (Truong-Hong and Laefer 2015; Truong-Hong et al. 2016). However, those scanners are relatively expensive (typically starting at $25,000) and need a flat base and clear line of site (Figure 1b), which may not be available. Moreover, as the scanner’s location is fixed during scanning, the line of sight nature of the technology may potentially result in occlusions where objects are located between the scanner and the target object or when the scene geometry causes self-shadowing (see Figure 2) [Hinks et al. 2009].

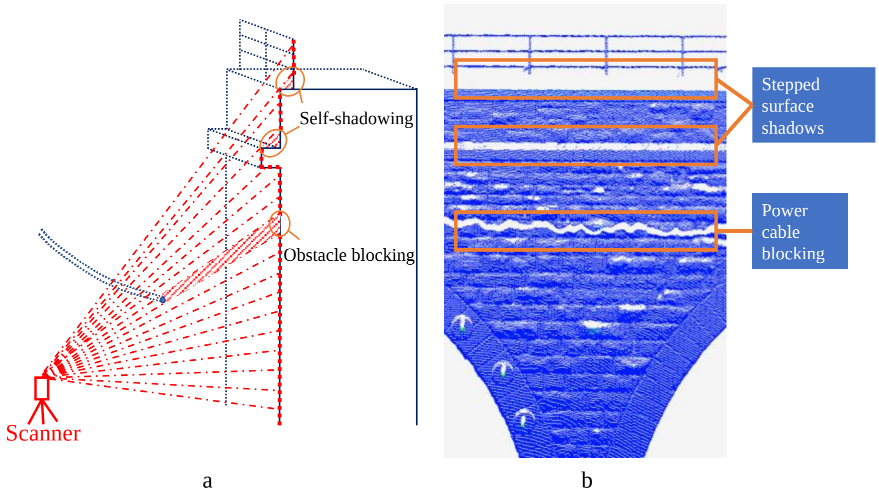

Fig. 2. Missing data phenomenon in TLS scans. (a) Schematic of occlusion and self-shadowing problem; (b) Point cloud from TLS data

Unmanned Aerial Vehicle (UAV) Inspection

As a possible alternative, UAV-based inspections can offer the combined advantages of robot inspection and remote sensor inspection. As such, the topic has received significant interest for baseline documentation and surface evaluation of bridges (Yin et al. 2015), roads (Díaz-Vilariño et al. 2016) and buildings (Fernandez Galarreta et al. 2014). Compared to traditional inspection methods, UAV-based inspection has clear advantages. Firstly, in hard to reach areas, such as cable towers and deck bottoms, UAV-based access is less restricted by distance and angle. So better site visibility and optimized views can be acquired (Kim et al. 2015), especially where computer-based path planning is employed to maximize data capture coverage (Bircher et al. 2015). Secondly, UAVs present a significant financial advantage. For example in 2015, Chan et al. (2015) introduced a UAV system for bridge inspection that employed an aerial light detection and ranging (LiDAR) sensor that cost about $6,000, which was less than a quarter of the cost of in-person methods. More recently, Byrne et al. (2017a) presented a solution to employ UAV-based aerial video footage for building surveying, with equipment costing less than $1,000. Thirdly, UAVs can carry a wide range of task-specific sensors, including RGB cameras, laser scanners, thermal cameras, hyperspectral cameras, and aperture radars, for different inspection purposes (Chen et al. 2016).

Until relatively recently, laser scanners were able to provide high quality 3D point clouds only with relatively expensive and heavy equipment needing to be mounted on fixed-wing UAVs (Wallace et al. 2012). This was problematic, as effective bridge inspection requires outstanding hovering capabilities and manoeuvrability around piers and even between trusses, which necessitates a small, multi-rotor UAV. Due to weight and expense, imagery has been favoured for UAV-based bridge inspection but not without difficulties. Kim et al. (2015) presented such a camera-based, UAV system for concrete bridge surface crack detection. In their research, a morphological algorithm was designed for detecting and measuring crack widths but resulted in a highly variable error (3%-50%). However, in this fast-changing field, significant improvements occur frequently in terms of both hardware and software. As an example, Escobar-Wolf et al. (2017) employed a thermal camera for under-surface delamination and hole detection. In their case study, they generated thermal and visible images for a 968 m^2 area, from which 14 m^2 of delamination was identified – an overall accuracy of about 95% compared to direct contact hammer sounding data. Based on the current technology and the applications of UAVs in bridge inspection, there are two aspects of aerial data collection that can improve results, which are considered as part of the proposed methodology:

1. Separation of the requirements and the necessary processes: Bridge inspection is requirement driven, with the desired information scope and type typically dictated by the

specific bridge. As such, every aerial data collection mission should start with the identification of the requirements to which any generic or proprietary process must be applied. The specified process forms the foundation of how to (1) achieve the desired data collection, (2) add value over traditional methods, and (3) maintain high safety standards during the execution.

2. Assessment of the flight process: Each operation is unique and comes with specific operational variables that must be considered to achieve a safe and legally compliant flight mission.

Methodology

To achieve a systematic and reliable bridge inspection, a UAV-based inspection framework is needed, as proposed in Figure 3. As will be explained in the following subsections, this involves four main tasks: (1) data acquisition; (2) 3D reconstruction; (3) quality evaluation of the 3D reconstruction; and (4) damage detection.

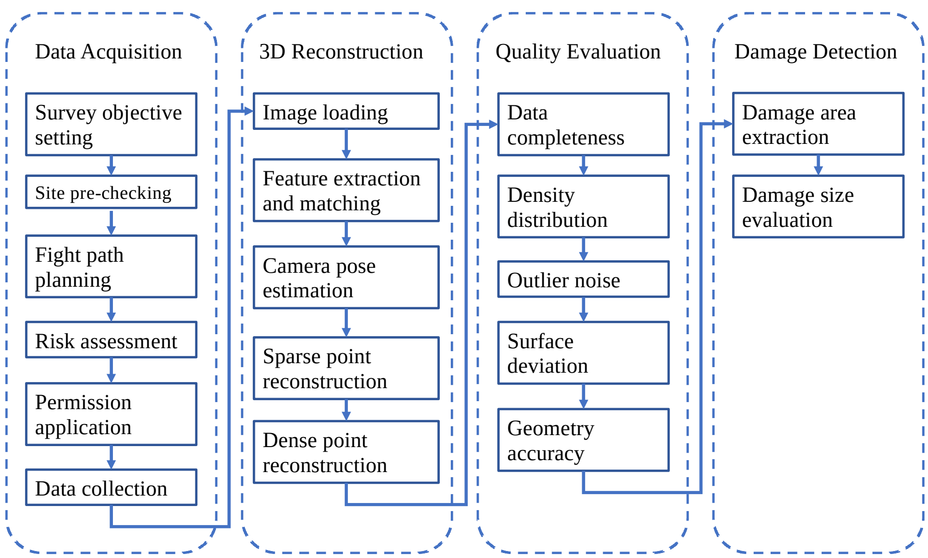

Fig. 3. Framework for UAV inspection

Data Acquisition

The task of data acquisition includes site pre-checking, fight plan drafting, risk assessment, permission application, and on-site data collection. Each step has its own requirements as introduced in the Table 1.

Table 1. Procedures for UAV inspection

Workflow	Steps
Survey objective setting	Determine which areas are to be covered and what information needs to be collected.
Site pre-checking	Become familiar with the basic geographical information of the target and its surroundings to know the traffic frequency of nearby roads and distances to those roads, surrounding buildings, and/or trees.
Fight planning	Choose the flight path – including the take-off locations, flight speeds and heights, distance to the object, camera settings, and emergency landing places. Check the weather to avoid windy and raining days, and avoid peak traffic hours.
Risk assessment	Reduce the risk of the accident by keeping a notable distance from the survey target, vehicular traffic, people, water, trees, power cables, and signal towers.
Permission application	Obtain permissions from the landowner or site manager and the aviation authority for the specified flight plan.
Data collection	Notify any potentially impacted populations about when the aerial survey will start. Follow the devised flight plan for data collection, if any emergency occurs, land the UAV safely.

Among the Table 1 steps, the flight path planning arguably has the strongest impact on the data quality, as it relates to light conditions, camera angle, offset distances, flight pattern, and degree of overlap between images (Chen et al. 2017). While overlapping rates are rarely reported and appear to be empirically selected, Paine and Kiser (2003) recommended 60% ± 5% for endlap and 30% ± 15% for sidelap.

To better explain the relationship between camera angle and distance, the terminology Ground Sampling Distance (GSD) is referred to in remote sensing as spatial resolution, which is used here to describe the image quality. The GSD equals the distance between the centre of two consecutive pixels on the target surface. Figure 4 shows the projection relationship of a simplified digital camera system. In an orthographic projection, the GSD will be the same in the field. In a tilt projection, the far end will have the maximum GSD value. This means that each pixel covers a larger area in the corner D than in corner A, and the edge DC will have the maximal GSD of the entire field of view (FOV). Figure 5 shows the relationship between the GSD value, the sensor size [horizontal sensor size (HSZ) times vertical sensor size (VSS)], the focal length (f), the working distance (WD) from the camera to the object, the camera tilt angle (αt) from the camera axis to the surface normal, and the resolution of the sensor [horizontal pixel numbers (HN) time vertical pixel numbers (VN)].

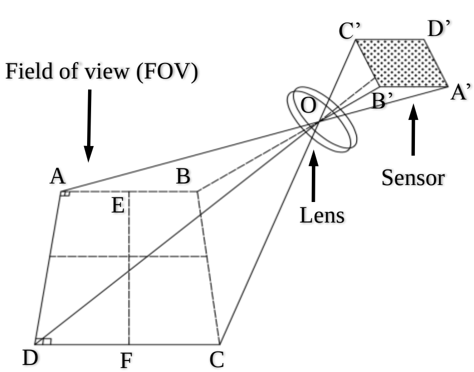

Fig. 4. Projection relationship 3D

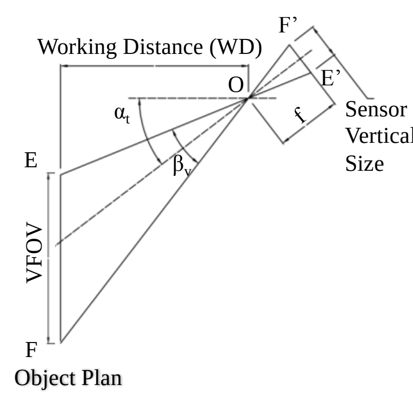

Fig. 5. Projection relationship two-dimensional (2D)

Based on the geometric relationship, the average GSD on the edge CD can be calculated by equation (1). The vertical camera view angle βv is defined in equation (2).

$$\mathrm{GSD}_{max} = \frac{WD \times \mathrm{HSS} \times \cos\frac{\beta_v}{2}}{f \times \mathrm{HN} \times \cos\left(\alpha + \frac{\beta_v}{2}\right)} \quad (1)$$

$$\beta_v = 2 \times \tan^{-1}\frac{VSS}{2\mathrm{f}} \qquad (2)$$

Ideally, a smaller GSD value is better, but the FOV value should be considered as well, as a larger FOV minimizes the number images required for data collection. The FOV value can be calculated by equation (3) [see Byrne et al. 2017b for a further discussion of this point].

$$\mathrm{FOV} = \frac{WD^2 \times HSS}{2f} \times \left(\frac{\cos\frac{\beta}{2}}{\cos\left(\alpha - \frac{\beta}{2}\right)} + \frac{\cos\frac{\beta}{2}}{\cos\left(\alpha + \frac{\beta}{2}\right)}\right) \times \left(\tan\left(\alpha + \frac{\beta}{2}\right) - \tan\left(\alpha - \frac{\beta}{2}\right)\right) \quad (3)$$

For inspections, most data acquisition parameters are related to the device and are unalterable, such as the sensor size, focal length, and pixel numbers. For example, with the DJI Phantom 4 UAV, the sensor size is 6.17mm x 4.55 mm, the focal length is fixed at 3.55 mm, and the pixel numbers are 4000 x 3000. Thus, the maximal GSD value and FOV value are only affected by the working distance and the tilt angle. Figure 6 demonstrates calculating the FOV vs GSD chart for DJI phantom 4, with respect to the tilt angle and offset distance. After calculation of the GSD and FOV, an appropriate working distance and tilt angle can be selected to match the surveying objective(s) for image collection. Once collected, imagery can be used for 3D model generation, as described in the next subsection.

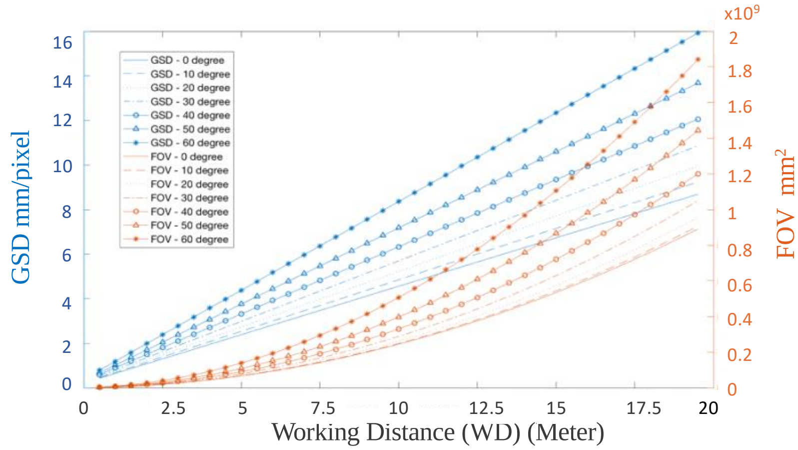

Fig. 6. FOV vs GSD

3D Reconstruction

Once imagery data are captured, they must be processed in a manner usable for the final application. Traditionally, conventional camera inspections have concentrated on individual 2D images, which precludes direct 3D location measurement and volumetric estimation (Eschmann et al. 2013). Further manipulation to generate a 3D point cloud can be achieved through the Structure from Motion (SfM) method, as first introduced by Ullman (1979). SfM utilizes images taken from at least two viewpoints. By detecting key points in each image, the geometric relationship between images can be calculated and used for triangulation, from which the depth information of key points is derived and placed into a unique coordinate system. The approach can be decomposed into (1) feature extraction and tracking, (2) pose estimation, (3) 3D point registration, and (4) surface reconstruction (Szeliski 2010). A scale-invariant feature transform (SIFT) [Lowe 2004], providing efficient feature extraction and bundle adjustment, was also applied to minimise the cumulative drift errors (Schonberger and Frahm 2016).

Those steps have been integrated in open source software like VisualSFM or OpenMVG and commercial software like PhotoScan and Pix4D and used for forest mapping (Wallace et al. 2016), geoscience surveying (Westoby et al. 2012), agriculture monitoring (Zarco-Tejada et al. 2014), and urban modelling (Byrne and Laefer 2016). With respect to bridges, Hallermann et al. (2016) presented a case study that illustrated the possibility of using UAVs for 3D bridge inspection. However, published work in this area tends not to report evaluations of the quality of the full reconstructed 3D point clouds, instead reporting evaluations only from further derived products (e.g. crack identification).

Data Quality Evaluation

Generally, 3D reconstructed point clouds include defects such as missing data. This is caused by line-of-site-based occlusions (Tagliasacchi et al. 2009), non-uniform data densities (Berger et al. 2014), inaccurate geometric positioning (Sargent, et al. 2007), surface deviations (Koutsoudis et al. 2014), and outlier-based noise (Cheng and Lau 2017). Each defect type is illustrated in Figure 7. Despite the common occurrence of these types of problems, specific metrics to evaluate UAV-generated 3D models have yet to be established. A review of 20 papers published between 2000 and 2017 related to UAV-based inspection with imagery based point clouds demonstrated that only three of them considered any evaluation beyond subjective visual fidelity. Of those Byrne et al. (2017b) proposed using inlier matching, as well as the final reconstruction, while Palmer et al. (2015) and Koutsoudis et al. (2014) evaluated geometric distance errors. Notably despite the rapidly growing popularity of UAV-based imagery 3D reconstructions, a broadly accepted set of standards for evaluating the resulting 3D models has yet to established. To overcome this deficit, the research herein will propose a rigorous evaluation method for assessing UAV-generated, 3D point clouds for the purpose of bridge inspection. For this, a series of functions has been designed to consider each possible defect within the data evaluation flow chart (Figure 8), as explained in the following sections. The results have been benchmarked against terrestrial laser scanner (TLS) data, as that technology is widely used in surveying and considered to be accurate to the centimetre level in building inspection (Quagliarini et al. 2017).

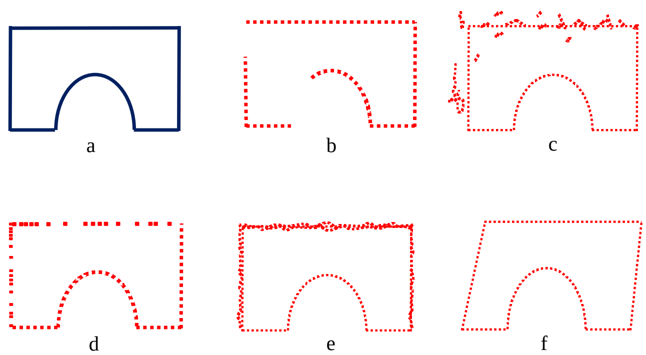

Fig. 7. Point cloud defects. (a) Real structure; (b) Incomplete data; (c) Outlier noise (d) Non-uniform density; (e) Surface deviation; (f) Geometric deformation

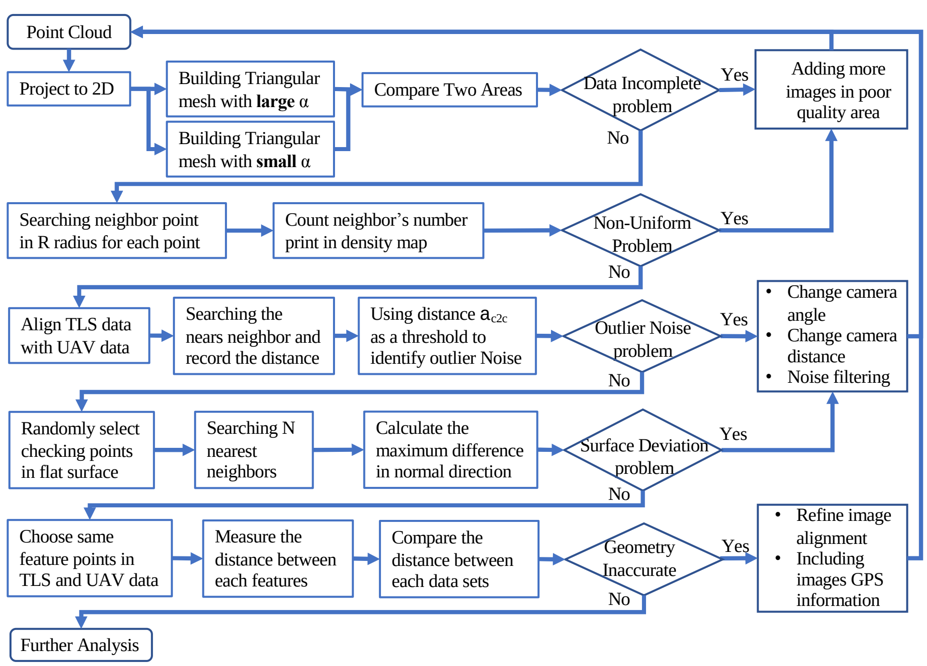

Fig. 8. Flow chart of data evaluation

Evaluating Incomplete Data

In terms of UAV-based reconstruction, the missing data problem persists in poorly overlapped areas (Figure 9a), especially for slim or narrow portions of the structures (e.g. railings in Figure 9b), since there are insufficient features for image matching. Increasing the extent of image overlap can minimize this problem.

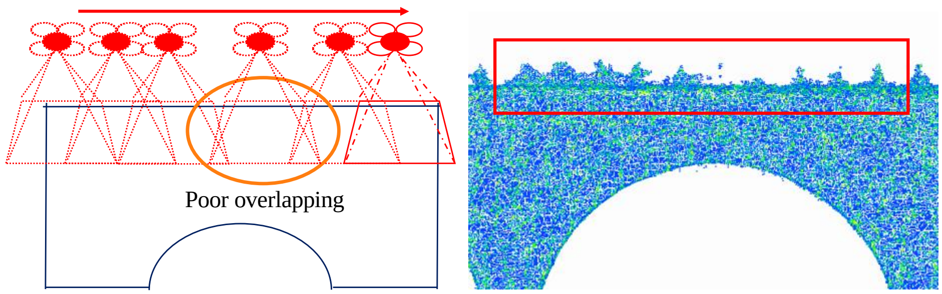

a b

Fig. 9. UAV-SFM data missing. (a) Poor overlapping; (b) Sample UAV data taken from 20m

For the purpose of quantifying the degree of data completeness, a 2D area evaluation method was designed. This involves first projecting the testing surface data (Figure 10a) onto their normal plane. Then, in the 2D projection plane, a triangular mesh is built between each point. The threshold α is applied here to control the searching radius for mesh generation. For any point C, within the radius α, if any neighbour points exist, a triangular mesh will be generated for area calculation. Thus, by controlling the threshold $\alpha p2p$, the area with and without incomplete coverage can be calculated. To choose an appropriate α, the average distance of any point to its nearest neighbours must be measured. In this algorithm, 5% of the points were randomly taken from the original data as querying points and used in a nearest neighbour searching (NNS) algorithm (Muja and Lowe, 2009) to find the closest point to each query point. Then, the average Euclidean distance (β_{ave}) and standard deviation (β_{std}) of all pairs of query points and their closest neighbours are calculated. If α is much larger than β_{ave}, then the incomplete area is included, as shown in Figure 10b. Although not entirely accurate, because this mesh fills all the holes and fully covers the structure, this meshed representation will be used as the ground truth for the purpose of evaluation. If the α_{p2p} value is close to β_{ave} and within $\pm\beta_{std}$, then the mesh will ignore the incomplete area and only represent the real data coverage, as shown in Figure 10c. By comparing these two meshes, the degree of coverage can be measured to a reasonable level.

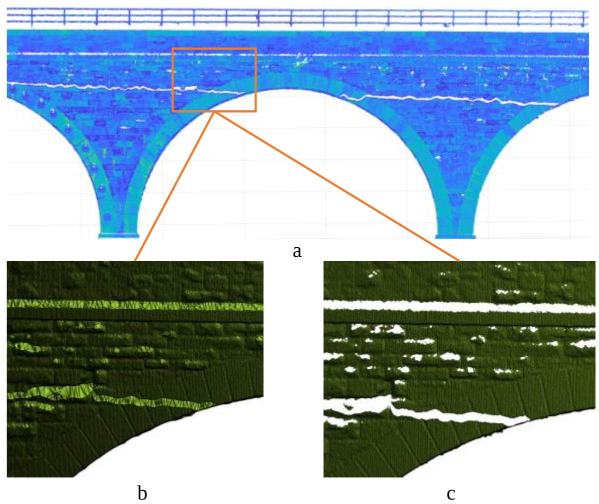

Fig. 10. Testing dataset (βave=0.02m, βstd=0.006m) b. Mesh with incomplete area (αp2p =0.2) c. Mesh without incomplete area (αp2p =0.025m)

Evaluating Non-uniform Distribution

A non-uniformly distributed point cloud may have insufficient points in low-density areas, which will cause problems for further analysis, such as point cloud simplification (Moenning and Dodgson 2003) or surface reconstruction (Huang et al. 2009). The point distribution can be measured easily by volume density. For each point, the number of neighbouring points in a spherical neighbourhood of a defined radius R can be counted and presented in a density map. As illustrated in Figure 11, point A has 4 neighbour points in the searching area within a radius R, while point B has 6 neighbours, and point C has 9.

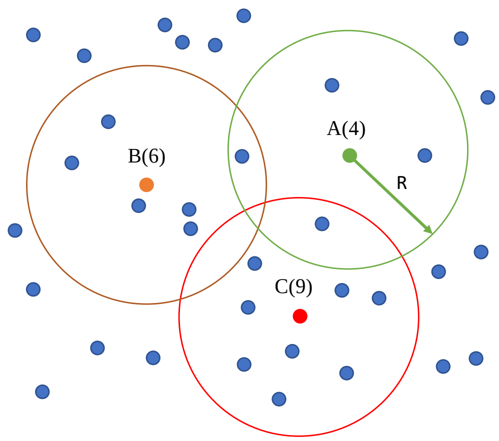

Fig. 11. Volume density

Evaluating Outlier Noise

Outlier noise usually appears around the boundary of the structure. One reason is that textureless backgrounds (like sky) tend to confuse SfM approaches. For example, the railing area in Figure 12 is poorly reconstructed, as the reconstruction algorithm treats the background (sky) as part of the front object (bridge). For example, as the camera failed to fully observe the area beneath the arch, many outliers appear around the border. Those outlier points will affect subsequent surface reconstruction and generate floating artefacts around the object. Additionally, shadows and large tilt angles weaken or hide the surface texture.

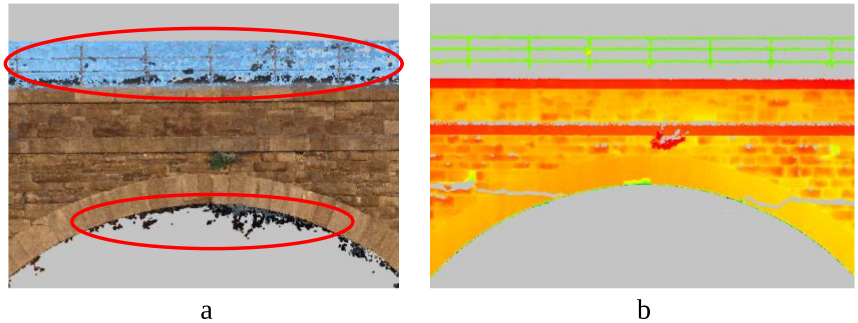

Fig. 12. Outlier Points comparison. (a) UAV dataset; (b) TLS dataset

As the outlier problem is more significant in the imagery, the TLS dataset is considered as the reference dataset and compared to the relative noise level in the UAV data. To do this, first the UAV data are aligned to the TLS data using the Iterative Closest Point (ICP) algorithm (Besl and McKay 1992). Then, the distance between specific points in each set is calculated. For each point in the UAV dataset, a search is undertaken for its nearest neighbour point in the TLS dataset, and the offset distance is recorded. An example of a cloud-to-cloud distance map is shown in Figure 13. By setting a threshold α_{c2c} to control the maximum distance, the outlier noise can be filtered out, as shown in red in Figure 13. Here, α_{c2c} equals the mean distance λ_{ave} plus two times the standard deviation λ_{std}. Using the total number of points to divide the outlier points number shows the percentage of outlier noise.

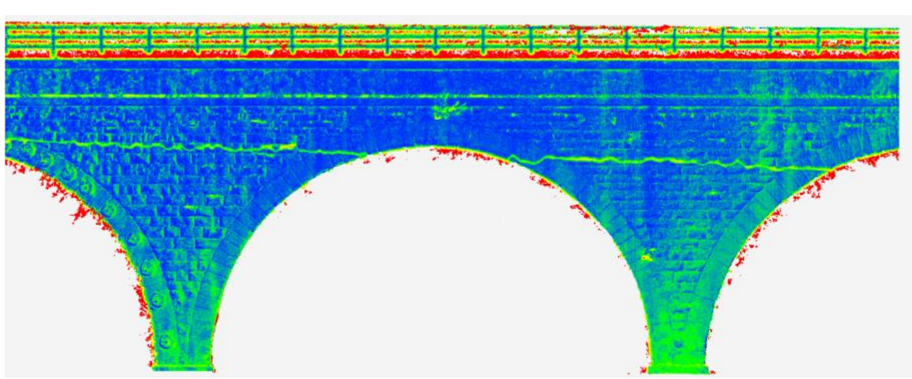

Fig. 13. Cloud to cloud distance map (λave=0.04, λstd=0.07, αc2c=0.18)

Evaluating Surface Deviation

Theoretically, a surface should contain only one layer of points. Thus, the thickness of points along a scanned surface should be close to zero, but the reality is otherwise. This is because the reconstruction mechanisms are not completely accurate. Specifically, some points will deviate from the real surface, which results in the point cloud surface presenting as if it is of a certain thickness, despite its true planar nature. The thickness will cause problems for further mesh generation, surface reconstruction, and retention of small details (Wolff et al. 2016). A method to evaluate the point cloud surface deviation level involves selecting a few checkpoints to measure the thickness and point distribution in the immediate neighbourhood. Choosing the checkpoint is best done from a flat surface to avoid incorporating surface changes in the deviation. An example is shown in Figure 14, where three checkpoints are selected within a defined neighbourhood of 1 cm^2 in the XY direction. The difference between Z-max and Z-min is the thickness at that location.

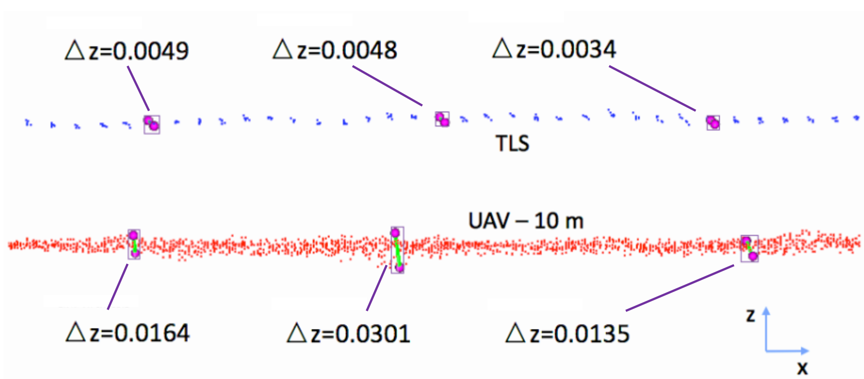

Fig. 14. Surface deviation

Evaluating Geometric Accuracy

Geometric accuracy is important for engineering inspection, especially for deformation monitoring and quantifiable damage assessment. One method to do this involves measuring the point-to-point distance of specified feature pairs (Koutsoudis et al. 2014). This requires choosing a few visually recognizable feature points (e.g. a corner or colour mark). By measuring the relative distance of the same feature pairs in the different datasets, the relative accuracy between the different datasets can be measured.

Damage Evaluation

Compared to image based 2D inspection, reconstructed 3D point clouds provide depth information for holes and cracks making volumetric damage calculation possible, which is important for structural health evaluation. To achieve that, the damaged area needs to be extracted from the dataset. This can be completed by means of manual segmentation or using an auto-clustering algorithm, such as K-means or DBSCAN. Within the extracted boundary, volume calculation can be done by filling the space with random points and generating a triangular mesh from which the volumetric calculation can be done.

Case Study

To demonstrate the proposed procedure, a field test was conducted of the Boyne Viaduct Bridge (Figure 15), located in Drogheda, Ireland. The bridge was selected because of its location beyond the restricted air space of Dublin Airport and its clear line of sight for TLS inspection. The bridge is 30m high, comprised of 15 masonry spans (12 on the south and 3 on the north side), as well as 3 girder spans of wrought-iron. After site pre-checking, risk assessment, and permission application (Table 1), arches No. 1 to No. 6 on the southern side were selected as the focus of the survey. Flight permission was not possible for arches No. 7 to No. 12 due to potential UAV-risks to pedestrian, vehicles, and the adjacent railway. Furthermore, the northern abutment was located on private property for which requested access was denied. The survey was conducted at 5:30 a.m.

of May of 2017 and lasted for 40 minutes. The TLS unit was located on the south bank where permission was obtainable.

Data Acquisition

UAV Data Collection

A relatively low end UAV in the form of a DJI Phantom 4 quadrotor (Figure 16) was employed with a 12-megapixel (4000x3000) digital camera. This commercial unit was augmented with a 3-axis stabilization gimbal. While more expensive UAVs and cameras are available, the purpose of this flight was to show the proposed framework in a real-life scenario.

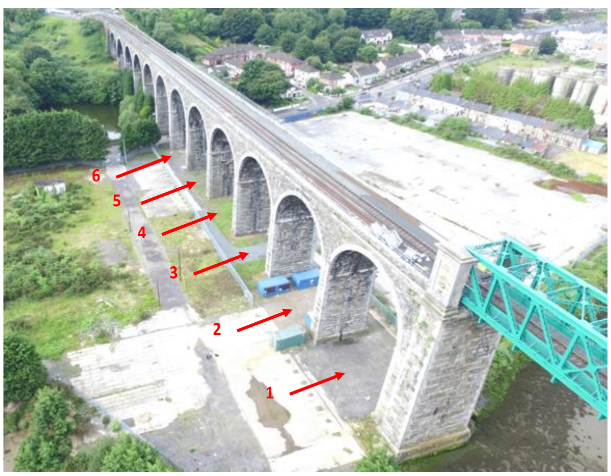

Fig. 15. Boyne Viaduct Bridge showing the south side of arches 1-12

Fig. 16. UAV showing the south side of arches 1-6

The flight trajectory was pre-designed as per Figure 17. On each side of the bridge's southern end, take offs A and B included 3 flight paths with angles ranging from 0º to 45º and offset distances of 20 m to 40 m (Table 2). To obtain additional details for surface deterioration, a third take off was undertaken. Arch No. 5 was selected as the target, because a small spalled area was manually identified during a ground-based pre-check. To document this area in a more detailed manner, 10 additional images were taken from a distance of 10 m away via take-off C. Using the chart in Figure 6, the GSD is less than 5 mm/pixel. A total of 295 images were acquired during the 3 flights, and all images were used for the 3D reconstruction. As ground-based access (for verification) was not possible from the north side, data collection efforts were concentrated on the bridge's southern side.

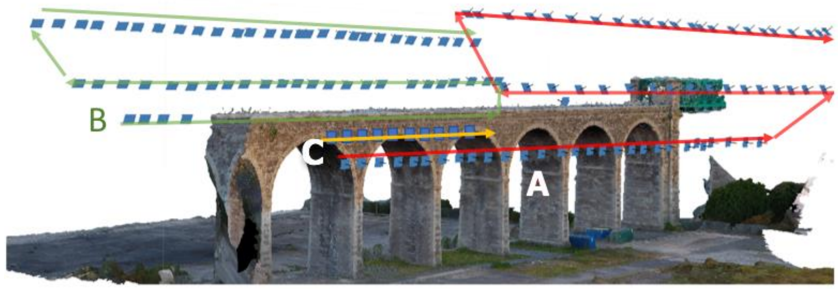

Fig. 17. Flight path on both sides (image showing south side of arches 1-6)

Table 2. Flight Information

Take off	Take-off location	Flight Time	Images	Distance	Height	Angle
			30	20 m	20 m	0°
A	South-east side	11 minutes	17	40 m	25 m	30°
			24	40 m	45 m	45°
			33	20 m	20 m	0°
B	South-west side	14 minutes	25	40 m	25 m	30°
			29	40 m	45 m	45°
C	South-east side	3 minutes	10	10 m	20 m	0°

TLS Data Collection

For collection of reference data, a Leica Scan Station P20 terrestrial laser scanner was used (Figure 18). The unit's resolution was set as 12.5 mm at 10 m resulting in a typical data density of 6400 pts/m^2. Scans were taken from 3 locations (see Figure 19) along the southeast portion of the bridge and required approximately 1.5 hours in total. As the bridge deck was not accessible, the terrestrial laser scan data only covered the side of the bridge.

Fig. 18. Terrestrial laser scanner

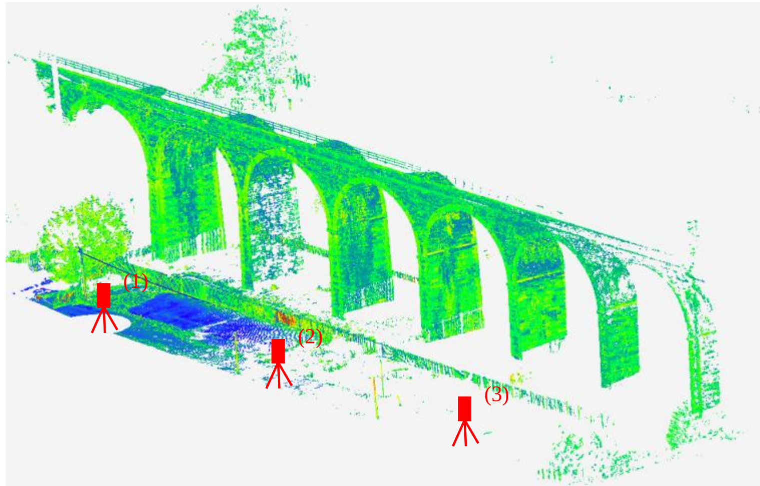

Fig. 19. Scanning location

3D Reconstruction

After data collection, the software Photoscan (Agisoft 2017) was applied to generate the 3D point cloud, including the 153 images from take offs 1 and 2. A Dell laptop with an Intel i7 processor (4 cores, 2.8 GHz), 16 Gb RAM was employed for the data processing. A total of 4 hours and 14 minutes was required to build a model from 24,404,204 points using UAV-20m (20 m was the closest distance to the object). Adding 10 extra images of arch No. 5 (taken from 10 m) increased the dataset to 24,802,421 points. This resulted in the UAV-10m model (closest distance to object 10 m) which required 5 hours 58 minutes of processing time. As each new image must be matched with all the previous ones in the data set, the additional time is disproportional to the amount of information added (i.e. less than a 2% increase in the number of points for nearly a 41% increase in processing time).

Quality Evaluation

To reduce the computing time of the evaluation, the data related to arch No. 5 (Figure 20) was manually segregated for the additional processing. The three subsets used as input for the evaluation are shown in Figure 21.

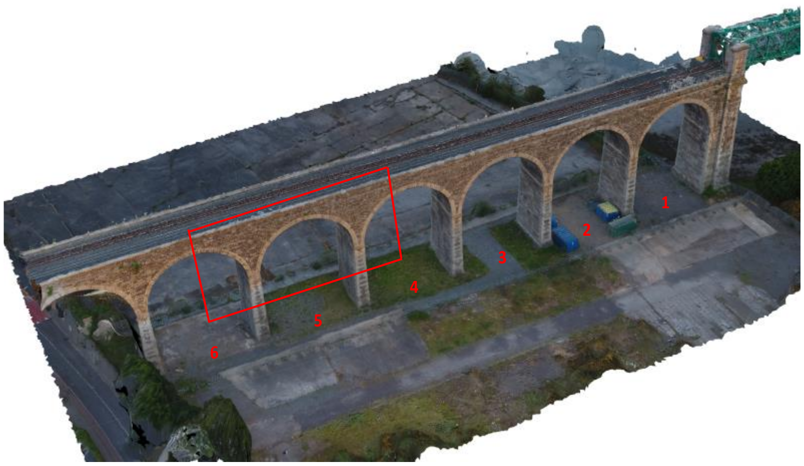

Fig. 20. Model UAV-20m

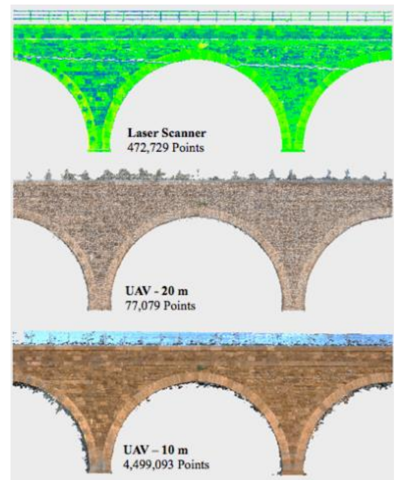

Fig. 21. Evaluation Section for Arch No. 5 (South Side)

Evaluation of Incomplete Data

The TLS dataset was used for defining the valid area of the structure. Calculating the coverage rate involved setting the threshold α_{p2p} to about 20 times larger than that of β_{ave} to obtain the ground truth and setting it equal to β_{ave}+ β_{std} to determine the real coverage. The results are shown in Table 3, with the UAV-10m dataset resulting in the best coverage rate at 93.46%. For the UAV-20m dataset, about 20% of the area was not covered, which largely corresponded to the missing data for the railing portion of the bridge which resulted insufficient feature matching in this area.

Table 3. Coverage Comparison

Datasets	βave	βstd	αp2p	Area m^2	Coverage
Ground Truth	0.0205	0.0064	0.4101	296.7946	100%
TLS	0.0205	0.0064	0.0269	239.6658	71.83%
UAV-10m	0.0078	0.0032	0.0109	277.3921	93.46%
UAV-20m	0.0507	0.0174	0.0681	239.6658	80.75%

Evaluation of Point Distribution

To evaluate the point distribution situation with a neighbourhood of a radius 0.05 m, the volume density was calculated for each point (see Figure 22). As expected, TLS point distribution was highly non-uniform, with portions of the bridge closer to the scanner captured more densely (e.g. the bottom left-hand corner) than those further afield. In contrast, the UAV datasets were more uniformly distributed but had more local density variation (as shown in the colour changes in the UAV density maps, especially near the bottom edges or the arches). The density of the 10 m dataset was higher than the 20 m dataset, with significant differences between the background and the rails, which can be used as a feature to remove the background noise.

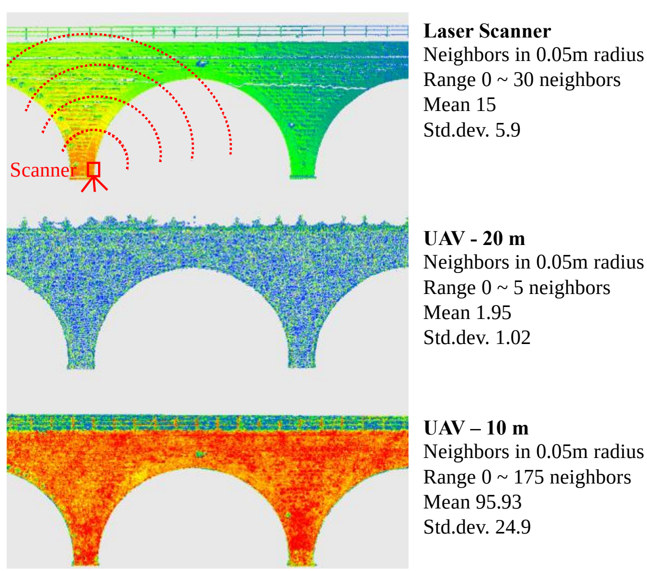

Fig. 22. Point density map

Evaluation of Outlier Noise

Using the method outlined in the Methodology section, the UAV dataset was aligned with the TLS data, and the outlier noise level for each UAV dataset was calculated (Table 4). The UAV-10m noise level was 4.52% – approximately 1/3rd less than that of the UAV-20m dataset (at 6.87%), which means adding close up images with more details can help reduce the outlier noise level in the reconstructed point cloud.

Table 4. Outlier Noise Evaluation

Datasets	λave	λstd	αc2c	Total Points	Outlier Points	Outlier Noise Percentage
UAV-10m	0.0456	0.0705	0.1866	4,296,232	194,068	4.52%
UAV-20m	0.0784	0.1146	0.3076	73,342	5,042	6.87%

Evaluation of Surface deviation

As previously mentioned, measuring surface deviation is easier on a flat surface. In the small, immediate neighbourhood around the checking points, the surface approximates a flat surface. Therefore, using that surface, 20 points were picked randomly for evaluation (Figure 23). The thickness of the UAV-based dataset was about three times greater than that of the TLS data meaning that the TLS data had fewer surface deviations and more closely captured the real surface geometry (Figure 24). Geometric accuracy is especially important for baseline documentation and crack tracking.

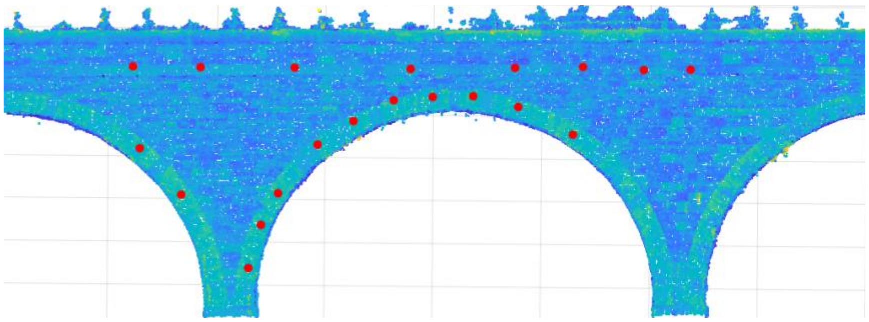

Fig. 23. Random checking points on flat surfaces

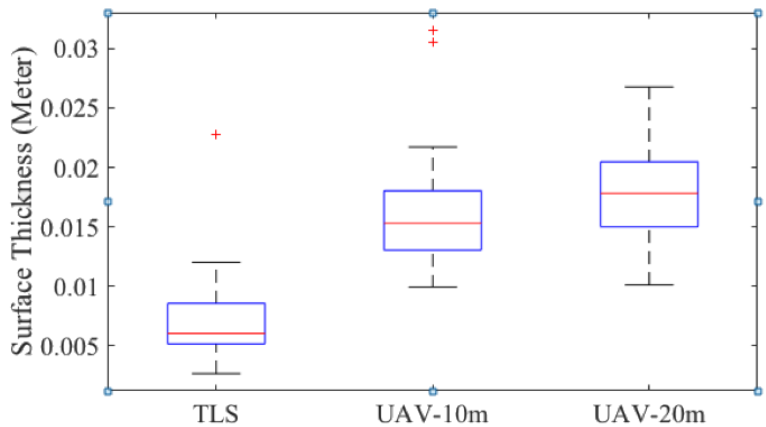

Fig. 24. Thickness distribution

Evaluation of Geometric Accuracy

Employing Koutsoudis et al.'s (2014) method for evaluation of geometric accuracy, the TLS data served as a reference data set against which to evaluate the UAV-based point cloud. To measure the point-to-point distance, three easily detectable features were selected. These were corner points at the bottom or top of the arch (Figure 25). As selecting the exact same points across datasets is unlikely, concepts from the "Guide to the Expression of Uncertainty in Measurement" (GUM) were applied (JCGM/WG 1). Each distance was measured 10 times, which was used to calculate the mean distance and the type A standard uncertainty at each location. Table 5 shows the geometric offset from the UAV-10m dataset with relative errors up to 0.4%, while the UAV-20m dataset had slightly more, with errors up to 0.97%.

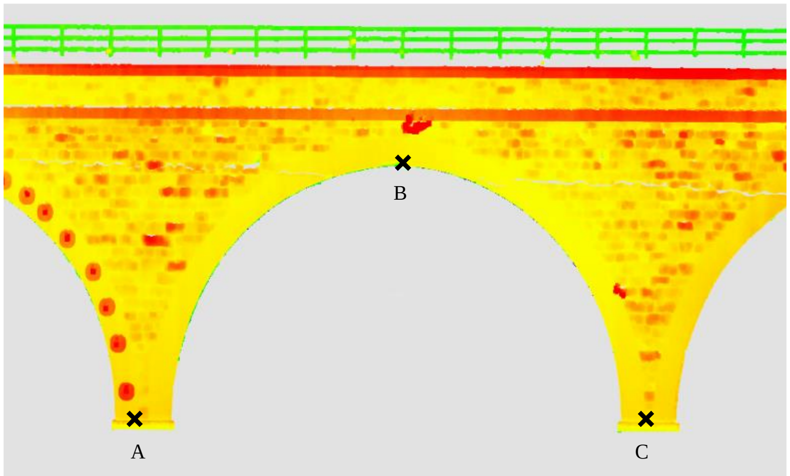

Fig. 25. Selected feature points

Table 5. Point-to-point distance (meter)

#	UAV-10			UAV-20			TLS		
	AB	BC	CA	AB	BC	CA	AB	BC	CA
1	14.103	13.611	20.666	14.295	13.723	20.744	14.176	13.517	20.685
2	14.080	13.590	20.668	14.343	13.776	20.799	14.175	13.567	20.672
3	14.160	13.590	20.666	14.252	13.625	20.729	14.206	13.521	20.672
4	14.126	13.605	20.674	14.141	13.625	20.747	14.187	13.567	20.673
5	14.120	13.626	20.657	14.295	13.723	20.747	14.197	13.566	20.681
6	14.120	13.578	20.657	14.430	13.723	20.599	14.181	13.564	20.704
7	14.110	13.576	20.691	14.206	13.669	20.760	14.192	13.566	20.681
8	14.156	13.563	20.636	14.345	13.625	20.801	14.179	13.561	20.692
9	14.142	13.523	20.670	14.220	13.679	20.725	14.175	13.567	20.673
10	14.149	13.556	20.657	14.294	13.723	20.747	14.183	13.585	20.692
Average	14.13	13.58	20.66	14.28	13.69	20.74	14.19	13.56	20.68
Std. Dev	1.24	1.08	3.22	1.29	1.11	3.24	1.26	1.07	3.22
Std. Err	0.39	0.34	1.02	0.41	0.35	1.02	0.40	0.34	1.02
Distance	14.1±0.4	13.6±0.3	20.7±1	14.3±0.4	13.7±0.4	20.7±1	14.2±0.4	13.6±0.3	20.7±1
Relative Err	0.06 (0.41%)	-0.02 (0.18%)	0.02 (0.28%)	-0.09 (0.68%)	-0.13 (0.97%)	-0.06 (0.28%)	—	—	—
Uncertainty	2.77%	2.52%	4.92%	2.88%	2.60%	4.95%	2.77%	2.52%	4.92%

Damage Evaluation

During the pre-check, spalling on arch No. 5 was observed by the inspector visually from the ground (Figure 26a). To measure the volume of the missing area (Figure 26b), the damage evaluation method discussed above was applied. First, the damaged boundary was manually extracted. Then, within the boundary, random points were generated to fill the space (Figure 26c). Finally, a triangular mesh was generated across the damaged part for 3D volume calculation (Figure 26d). The results are shown in Table 6 with only a 3.97% difference from the UAV-10m dataset, and a 25% difference from the UAV-20m dataset, thereby showing the critical importance of having high quality data in areas of damage.

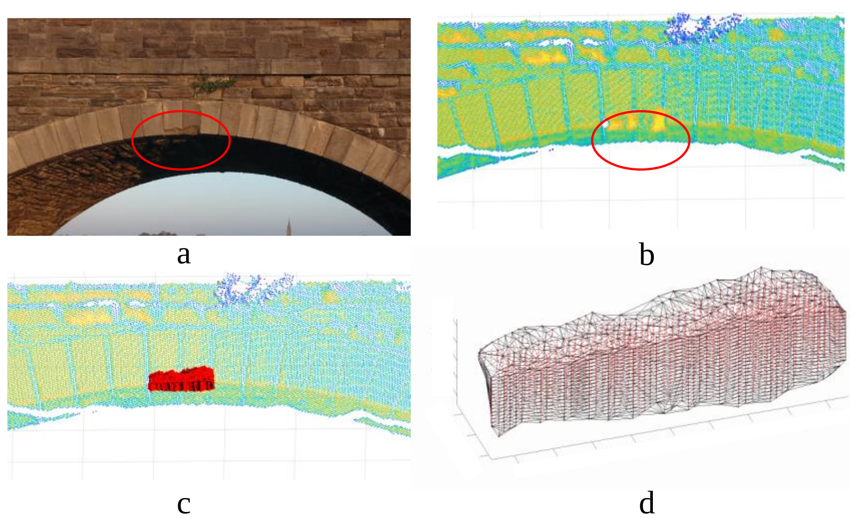

Fig. 26. Damage and volume evaluation of spalled brick of south side of arch No. 5. (a) Image data; (b) Point cloud data; (c) Filling of the damaged area with points; (d) Resulting volume of filling points

Table 6. Volume accuracy evaluation

	Volume	Error
TLS	0.0151 m3	-
UAV-10m	0.0157 m3	3.97%
UAV-20m	0.0189 m3	25.2%

Discussion

As mentioned above, the possibility of using UAVs for bridge inspection has been demonstrated in other studies. While much of the focus of that work centers on using high-end equipment to achieve better results, this is not necessarily so. For example, Katz (2018) reported the output of the relatively low-end DJI phantom series (as was used in the study herein) as comparable to a $70,000 Trimble unit with land-surveyor accuracy levels. Nonetheless, point clouds generated by the UAV-SfM method are generally less accurate than the TLS data. For example, while Slocum and Parrish (2017) showed that, under idealized conditions, UAV-SfM inspection accuracy can be in the range of 2.6mm to 32.2 mm, field experiments have shown that 3D distance measurement errors are more typically at the sub-meter level (Mosbrucker et al. 2017). Similarly, under idealized conditions, sales brochures claim that TLS can achieve mm level accuracy, but field experiments ultimately demonstrate accuracy at the centimeter level (Quagliarini et al. 2017), which is a slight, but notable improvement upon the sub-meter accuracy of UAV-SfM in the field.

However, accuracy is only one aspect of a quality dataset appropriate for inspection. There are also considerations of direct costs, scheduling issues, and access. For example, in the case study presented herein, the UAV equipment costs were less than 3% of that of the TLS ($2500 vs $103,000), and the on-site survey time was 33% (1 hour for UAV and 3 hours for TLS (Table 7).

Table 7. Comparison of UAV to TLS inspection

	UAV	TLS (Leica P-20)
Equipment and software costs	$2,500	$103,000*
Data Collection Time	<1 h	3 h
Data Processing Time	4h-1day	1h
Data Completeness	>80%	71.83%
Point Distribution	Well distributed	Radially distributed
Outlier Noise level	High	Low
Surface Deviation	High	Low
Geometry Accuracy	Centimetre Level	Millimetre level

*Relatively high quality units can be obtained for as little as $25,000

While these factors are important, for bridge projects access issues can predominate. Although the TLS data are more accurate, the scanner could only be set on bank. As mentioned before, the TLS data will cause a radial distribution problem in this situation. The data quality for the mid-span of the bridge will be relative poor, as it is far from the scanner and negatively impacted by the angle of incidence caused by the scanner position (Laefer et al. 2009). Positioning can also cause over-estimation of crack widths and lengths (Laefer et al. 2010) and has some strong practical limits based on positioning and beam size, even from only 15 m (Laefer et al. 2014). Additionally, line-of-site obstacles and uneven surfaces will interfere with complete coverage in the TLS dataset. The offset distance and angle of incidence has also been shown to compromise the data damage collection process. In contrast UAV-based 3D reconstruction method can easily overcome those problems and generate a full covered uniform point cloud with thoughtful pre-flight path planning.

Unfortunately, there are also disadvantages to UAV-based inspection. In the case herein, the UAV-based point cloud had a higher noise level than the TLS-based one, which was reflected in a more than 3 times higher deviation in the structure surface and marginally more outlier points (more than 4.52%). Additionally, narrow features make key point matching difficult using an SfM method, which will cause problems for bridge cable or truss inspection. Moreover, the 3D reconstruction process is more time-consuming than the TLS post-processing – spanning from a few hours to several days for the point cloud generation for each of the 3 flights versus only a single hour for the TLS data.

Conclusions

With respect to bridge inspection, this paper introduced a blended UAV-SfM method for imagery acquisition and 3D reconstruction. A case study for a major bridge in Dublin, Ireland was presented, and the proposed UAV-SfM method was compared with TLS-based inspection. A series of data evaluation methods were proposed to evaluate the point cloud performance in data completeness, density distribution, outlier noise level, surface deviation and geometry accuracy. In general, the study demonstrated that the UAV-SfM method can offer significant advantages in equipment cost, surveying time, point distribution, and ultimate data coverage. However, problems remain including high noise levels, low geometry accuracy and long post-processing times.

To solve these problems, future research will need to focus on optimizing 3D reconstruction algorithms and developing better noise removal techniques. Possible solutions could involve feature extraction algorithms that incorporate UAV position and orientation based on internal Global Position System (GPS) data and inertial measurement units, which could involve applying a weighting function to emphasize target features and de-emphasize items likely to be in the background (e.g. ground and sky) based on the proximity and focal area. Noise may similarly be removed through objective-based clustering algorithms.

Acknowledgments

This project was made possible through the generous support of the European Union’s Horizon 2020 Research and Innovation programme under the Marie Skłodowska-Curie grant 642453.

References

AASHTO (American Association of State Highway and Transportation Officials). (1970). Manual for Maintenance Inspection of Bridges, vol. 19705. AASHTO: Washington, DC, USA. <http://onlinemanuals.txdot.gov/txdotmanuals/ins/aashto_inspection_manuals.htm#6.>

Agisoft. (2017). “Agisoft PhotoScan.” <http://www.agisoft.com/> (Feb. 20, 2018)

Berger, M., Alliez, P., Tagliasacchi, A., Seversky, L. M., Silva, C. T., Levine, J. A. and Sharf, A. (2014). “State of the Art in Surface Reconstruction from Point Clouds.” *Eurographics 2014 -- State of the Art Reports*, 1(1), 161-185, 10.2312/egst.20141040

Besl, P.J., and McKay, N. D. (1992). “A Method for Registration of 3-D Shapes.” *IEEE Transactions on Pattern Analysis and Machine Intelligence*, 14(239–56), 10.1109/34.121791.

Bircher, A., Alexis, K., Burri, M., Oettershagen, P., Omari, S., Mantel, T., and Siegwart, R. (2015). “Structural Inspection Path Planning via Iterative Viewpoint Resampling with Application to Aerial Robotics.” *International Conference on Robotics and Automation, IEEE*, Piscataway, 6423–30, 10.1109/ICRA.2015.7140101.

Byrne, J., and Laefer, D. (2016). “Variables Effecting Photomosaic Reconstruction and Ortho-Rectification from Aerial Survey Datasets.” *arXiv Preprint*, arXiv:1611.03318.

Byrne, J., Laefer, D. F. and O’Keeffe, E. (2017a). “Maximizing Feature Detection in Aerial Unmanned Aerial Vehicle Datasets.” *Journal of Applied Remote Sensing*, 11(2), 1–2, 10.1117/1.JRS.11.025015.

Byrne, J., O’Keeffe, E., Lennon, D., and Laefer, D. F. (2017b). “3D Reconstructions Using Unstabilized Video Footage from an Unmanned Aerial Vehicle.” *Journal of Imaging*, 3(2), 15, 10.3390/jimaging3020015.

Chan, Br., Guan, H., Jo, J., and Blumenstein, M. (2015). “Towards UAV-Based Bridge Inspection Systems: A Review and an Application Perspective.” *Structural Monitoring and Maintenance*, 2(3), 283–300, 10.12989/smm.2015.2.3.283.

Chen, S., Laefer, D. F., Byrne, J., and Natanzi, A. S. (2017). “The Effect of Angles and Distance on Image-Based, Three-Dimensional Re-Constructions.” *Proc. European Safety and Reliability ESREL2017*, Taylor & Francis, Abingdon, UK, 2757–61.

Chen, S., Laefer, D. F., and Mangina, E. (2016). “State of Technology Review of Civilian UAVs.” *Recent Patents on Engineering*, 10(3), 160–74, 10.2174/1872212110666160712230039.

Cheng, S.-W., and Lau, M.-K. (2017). “Denoising a Point Cloud for Surface Reconstruction.” *arXiv Preprint*, arxiv:1704.04038v1.

Díaz-Vilariño, L., González-Jorge, H., Martínez-Sánchez, J., Bueno, M., and Arias, P. (2016). “Determining the Limits of Unmanned Aerial Photogrammetry for the Evaluation of Road Runoff.” *Measurement*, 85, 132–41, 10.1016/j.measurement.2016.02.030.

Eschmann, C., Kuo, C.M., Kuo, C.H., and Boller, C. (2013). “High-Resolution Multisensor Infrastructure Inspection With Unmanned Aircraft Systems.” *International Archives of* *the Photogrammetry, Remote Sensing and Spatial Information Sciences*, XL-1/W2, 125–29, 10.5194/isprsarchives-XL-1-W2-125-2013.

Escobar-wolf, R., Oommen, T., Brooks, C. N., Dobson, R. J., and Ahlborn, T. M. (2017). "Unmanned Aerial Vehicle (UAV)-Based Assessment of Concrete Bridge Deck Delamination Using Thermal and Visible Camera Sensors: A Preliminary Analysis." *Research in Nondestructive Evaluation*, 1-16, 10.1080/09349847.2017.1304597.

Fernandez Galarreta, J., Kerle, N., and Gerke, M. (2014). "UAV-Based Urban Structural Damage Assessment Using Object-Based Image Analysis and Semantic Reasoning." *Natural Hazards and Earth System Sciences Discussions*, 2(9), 5603–45, 10.5194/nhessd-2-5603-2014.

Hallermann, N., and Morgenthal, G. (2016). "From Aerial Photography to 3-Dimensional Inspection of Bridges." *Proc. IABSE Conference Guangzhou 2016: Bridges and Structures Sustainability-Seeking Intelligent Solutions*, International Association for Bridge and Structural Engineering, Zurich, 546–53, 10.2749/222137816819258898.

Hassanalian, M, and Abdelke, A. (2017). "Classifications, Applications, and Design Challenges of Drones: A Review." *Progress in Aerospace Sciences*, 91(May), 99–131, 10.1016/j.paerosci.2017.04.003.

Hinks, T., Carr, H., and Laefer, D. F. (2009). "Flight Optimization Algorithms for Aerial LiDAR Capture for Urban Infrastructure Model Generation." *Journal of Computing in Civil Engineering*, 10.1061/(ASCE)0887-3801(2009)23:6(330).

Huang, H., Li, D., Zhang, H., Ascher, U., and Cohen-Or, D. (2009). "Consolidation of Unorganized Point Clouds for Surface Reconstruction." *ACM Transactions on Graphics (TOG)*, 28(5), 176, 10.1145/1618452.1618522.

Jahanshahi, M. R., Masri, S. F., and Sukhatme, G. S. (2011). “Multi-Image Stitching and Scene Reconstruction for Evaluating Defect Evolution in Structures.” *Structural Health Monitoring*, 10(213), 643–57, 10.1177/1475921710395809.

JCGM/WG 1 (Working Group 1 of the Joint Committee for Guides in Metrology). (2008). "Evaluation of Measurement Data — Guide to the Expression of Uncertainty in Measurement." *JCGM 100:2008*, Online. <https://www.bipm.org/utils/common/documents/jcgm/JCGM_100_2008_E.pdf>

Katz, Daniel. (2018). “Distinctive Image Features from Scale-Invariant Keypoints.” *Commercial UAV News*, May 16. <https://www.expouav.com/news/latest/surveyors-and-other-professional-drone-operators-should-be-focused-on-accuracy-and-reliability/>.

Kim, J.-W., Kim, S.-B., Park, J.-C. and Nam, J. -W. (2015). “Development of Crack Detection System with Unmanned Aerial Vehicles and Digital Image Processing.” *Proc. Advances in Structure Engineering and Mechanics*, Incheon, Korea, 1–11.

Koutsoudis, A., Vidmar, B., Ioannakis, G., Arnaoutoglou, F., Pavlidis, G., and Chamzas, C. (2014). “Multi-Image 3D Reconstruction Data Evaluation.” *Journal of Cultural Heritage,* 15(1), 73–79, 10.1016/j.culher.2012.12.003.

Laefer, D.F., Fitzgerald, M., Maloney, E.M., Coyne, D., Lennon, D., and Morrish, S. (2009). “Lateral Image Degradation in Terrestrial Laser Scanning Author(s).” *Structural Engineering International*, 19(2), 184–89, 10.2749/101686609788220196.

Laefer, D.F., Gannon, J. and Deely, E. (2010). "Reliability of crack detection for baseline condition." *Journal of Infrastructure Systems*, 16(2), 129-137.

Laefer, D.F., Truong-Hong, L., Carr, H. and Singh, M. (2014). "Crack detection limits in unit based masonry with terrestrial laser scanning." *NDT&E International*, 62, 66-76.

Lowe, D.G. (2004). “Distinctive Image Features from Scale Invariant Keypoints.” *Int’l Journal of Computer Vision*, 60(2), 91–110, 10.1023/B:VISI.0000029664.99615.94.

Lueker, M., and Marr, J. (2014). “Scour Monitoring Technology Implementation.” *MN/RC 2014-37,* Minnesota Department of Transportation, St. Paul, MN.

Moenning, C., and Dodgson, N.A. (2003). “A New Point Cloud Simplification Algorithm.” *Proc. 3rd IASTED International Conference on Visualization, Imaging, and Image Processing,* ACTA Press, Calgary, 1027-33.

Mosbrucker, A.R., Major, J.J., Spicer, K.R., and Pitlick, J. (2017). “Camera System Considerations for Geomorphic Applications of SfM Photogrammetry.” *Earth Surface Processes and Landforms,* 42(6), 969–86, 10.1002/esp.4066.

Muja, M., and Lowe, D.G. (2009). “Fast Approximate Nearest Neighbors with Automatic Algorithm Configuration.” *Proc. VISAPP International Conference on Computer Vision Theory and Applications,* Scitepress, Setubal, Portugal, 331–40.

Nishimura, S., Kimoto, K., Abe, A., and Okazawa, T. (2012). “Development of a Hybrid Camera System for Bridge Inspection.” *Proc. Sixth International IABMAS Conference,* Taylor & Francis, Abingdon, UK, 2197–2203.

Paine, D.P., and Kiser, J.D. (2003). *Aerial photography and image interpretation*. John Wiley & Sons, Hoboken, NJ.

Palmer, L. M., Franke, K. W., Martin, R. A., Sines, B. E., Rollins, K. M. and Hedengren, J. D. (2015). “The Application and Accuracy of Structure from Motion Computer Vision Models with Full- Scale Geotechnical Field Tests.” *IFCEE 2015*, 2432–41, 10.1061/9780784479087.225.

Quagliarini, E., Clini, P., and Ripanti, M. (2017). “Fast , Low Cost and Safe Methodology for the Assessment of the State of Conservation of Historical Buildings from 3D Laser Scanning : The Case Study of Santa Maria in Portonovo (Italy).” *Journal of Cultural Heritage*, 24, 175–83, 10.1016/j.culher.2016.10.006.

RAIU (Railway Accident Investigation Unit). (2010). “Malahide Viaduct Collapse on the Dublin to Belfast Line, on the 21 St August 2009.” *Investigation Report No. 2010 – R004*, RAIU, Blackrock, Ireland.

Sargent, I., Harding, J., and Freeman, M. (2007). “Data Quality in 3D: Gauging Quality Measures from Users’ Requirements.” *International Archives of Photogrammetry, Remote Sensing and Spatial Information Sciences*, 36(2/C43), 8.

Schonberger, J.L., and Frahm, J.-M. (2016). “Structure-from-Motion Revisited.” In *Proceedings of the IEEE Conference on Computer Vision and Pattern Recognition*, 4104–13.

Slocum, R.K., and Parrish, C.E. (2017). “Simulated Imagery RenderingWorkflow for UAS-Based Photogrammetric 3D Reconstruction Accuracy Assessments.” *Remote Sensing*, 9(936), 1–19, 10.3390/rs9040396.

Sterritt, G. (2009). “Review of Bridge Inspection Competence and Training Project Report.” *Project: UG637*, UK Bridges Board, London, UK.

Szeliski, R. (2010). *Computer Vision: Algorithms and Applications.* Springer-Verlag, London, UK, 10.1007/978-1-84882-935-0.

Tagliasacchi, A., Zhang, H., and Cohen, D. (2009). “Curve Skeleton Extraction from Incomplete Point Cloud.” *ACM Transactions on Graphics*, 27(3), 1–10, 10.1145/1531326.1531377.

Truong-Hong, L., Falter, H., Lennon, D., and Laefer, D. F. (2016). "Framework for Bridge Inspection with Laser Scanning." *Proc. EASEC-14 Structural Engineering and Construction*, Ho Chi Minh City, Vietnam, 6 - 8 January 2016, 1–9.

Truong-Hong, L., and Laefer, D. F. (2015). "Documentation of Bridges by Terrestrial Laser Scanner." In *IABSE Symposium Report (Vol. 105, No. 19)*, International Association for Bridge and Structural Engineering, 1–8.

Ullman, S. (1979). "The Interpretation of Structure from Motion." *Proceedings of the Royal Society of London, Series B, Biological Sciences*, 203(1153), 405–26.

Wallace, L., Lucieer, A., Turner, D., and Vop, P. (2016). "Assessment of Forest Structure Using Two UAV Techniques: A Comparison of Airborne Laser Scanning and Structure from Motion (SfM) Point Clouds." *Forests*, 7(62), 1–16, 10.3390/f7030062.

Wallace, L., Lucieer, A., Watson, C., and Turner, D. (2012). "Development of a UAV-LiDAR System with Application to Forest Inventory." *Remote Sensing*, 4(6), 1519–43, 10.3390/rs4061519.

Westoby, M. J., Brasington, J., Glasser, N. F., Hambrey, M. J., and Reynolds, J. M. (2012). "'Structure-from-Motion' Photogrammetry: A Low-Cost, Effective Tool for Geoscience Applications." *Geomorphology*, 179, 300–314, 10.1016/j.geomorph.2012.08.021.

Wolff, K., Kim, C., Zimmer, H., Schroers, C., Botsch, M. and Sorkine-hornung Alexander, O. (2016). "Point Cloud Noise and Outlier Removal for Image-Based 3D Reconstruction." *Proc., 2016 Fourth International Conference on 3D Vision Point*, IEEE, Piscataway, 118–27, 10.1109/3DV.2016.20.

Yin, Z., Seto, C. and Mao, Y. (2015). “Develop a UAV Platform for Automated Bridge Inspection.” *Report No. 25-1121-0003-295, Missouri University of Science and Technology*, Rolla, MO.

Zarco-Tejada, P. J., Diaz-Varela, R., Angileri, V., and Loudjani, P. (2014). “Tree Height Quantification Using Very High Resolution Imagery Acquired from an Unmanned Aerial Vehicle (UAV) and Automatic 3D Photo-Reconstruction Methods.” *European Journal of Agronomy*, 55, 89–99, 10.1016/j.eja.2014.01.004.